Corrosion Science 123 (2017) 209–216

Contents lists available at ScienceDirect

Corrosion Science

journal homepage: www.elsevier.com/locate/corsci

Relationship between Ni release and cytocompatibility of Ni-Ti-O nanotubes prepared on biomedical NiTi alloy

Yanlian Liu[a], Zhiguo Ren[a], Long Bai[a], Mingxiang Zong[a], Ang Gao[b], Ruiqiang Hang[a,*], Husheng Jia[a], Bin Tang[a], Paul K. Chu[b]

[a] Research Institute of Surface Engineering, Taiyuan University of Technology, Taiyuan 030024, China
[b] Department of Physics and Materials Science, City University of Hong Kong, Tat Chee Avenue, Kowloon, Hong Kong, China

ARTICLE INFO

Keywords:
Nickel-titanium alloy
Anodization
Annealing
Corrosion
Cytocompatibility

ABSTRACT

To elucidate the relationship between Ni release and cytocompatibility of NiTi alloy, Ni-Ti-O nanotubes (NTs) are produced on its surface by anodization followed by annealing. The NiTi control has higher corrosion current density but releases less Ni than anodized samples, suggesting chemical dissolution of the NTs also contributes to Ni release. Although the annealed NTs release more Ni than that of NiTi control, they possess similar cytocompatibility. In addition, cytocompatibilitiy of the NTs with similar surface properties but have different Ni release levels is also comparable. These results suggest the amount of released Ni has little influence on the cytocompatibility.

1. Introduction

The nearly equiatomic nickel-titanium (NiTi) alloy is widely used in biomedical field because of its unique shape memory effect, superlasticity, and other desirable attributes [1–5]. However, release of Ni ions from the material into the human body causes health concerns. Although Ni is one of the essential trace elements, excessive amount of Ni is toxic, allergic, and even carcinogenic [6]. When exposed to human body fluids, the NiTi alloy suffers from electrochemical corrosion, during which process metallic Ni is converted to the ionic form and released from the material. Although the NiTi alloy is spontaneously covered with an amorphous oxide layer in an oxidizing environment, the layer is normally too thin and has poor self-healing ability to effectively suppress electrochemical corrosion and Ni release [7]. Accordingly, various surface modification techniques such as electrochemical treatment [8,9], excimer laser treatment [10], chemical etching [11], heat treatment [11,12], ion implantation [13–16], Fenton's oxidation [17], laser and electron beam irradiation [18], and magnetron sputtering [19] have been implemented to overcome the shortcomings of the native oxide layer, enhance the corrosion resistance, reduce Ni release, and improve the cytocompatibility. Nevertheless, these techniques not only reduce the release amount of Ni, but also alter the morphology, microstructure, and chemical composition of the surface of the NiTi alloy and so the definite relationship between Ni release and cytocompatibility cannot be drawn.

An emerging surface modification technique for NiTi alloy is anodization in a fluoride (F)-containing ethylene glycol (EG) electrolyte and this process can generate a well-defined nanotubular structure [20]. The method is promising for the following several reasons. First of all, it is cost effective and secondly, the solution-based approach is especially suitable for the devices with a complex shape. Thirdly, the nanotubes (NTs) with proper dimensions can enhance the functions of a variety of cells and fourthly, the NTs can serve as carriers for local delivery and release of various drugs [21–23]. Our previous work shows that Ni-Ti-O NTs with different size can be fabricated on the NiTi alloy by adjusting the anodization parameters [24] and an ensuing study indicates that the corrosion resistance, Ni release, and cycocompatibility of the NTs depends on their size [25]. Long NTs with a large diameter have poorer corrosion resistance and release more Ni ions than smaller ones, but larger NTs possess better cytocompatibility. Since NTs with different size possess the similar microstructure and chemical composition, the amount of released Ni and size may be the two key parameters in determining the cytocompatibility.

In this work, Ni-Ti-O NTs with the same size but different Ni release levels are prepared to elucidate the role of Ni release in the cytocompatibility of the NiTi alloy. The anodized samples are annealed at different temperature to investigate the morphology, microstructure, chemical composition, corrosion behavior, Ni release, and cytocompatibility of the NTs. The NTs annealed at the proper temperature possess the same morphology, microstructure, and chemical composition thus offering the suitable platform to investigate the relationship between Ni release and cytocompatibility.

* Corresponding author.
E-mail address: hangruiqiang@tyut.edu.cn (R. Hang).

http://dx.doi.org/10.1016/j.corsci.2017.05.006
Received 6 August 2016; Received in revised form 27 April 2017; Accepted 6 May 2017
Available online 10 May 2017
0010-938X/

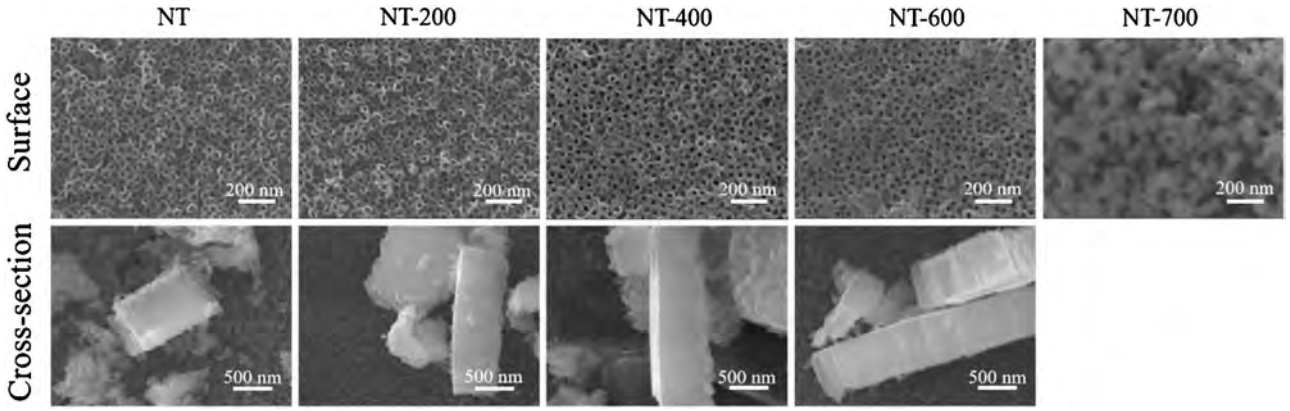

Fig. 1. Surface and cross-sectional FE-SEM images of the as-anodized (NT) and annealed Ni-Ti-O NTs (NT-200, NT-400, NT-600, and NT-700). NT-200: NTs annealed at 200 °C for 2 h; NT-400: NTs annealed at 400 °C for 2 h; NT-600: NTs annealed at 600 °C for 2 h; NT-700: NTs annealed at 700 °C for 2 h. The nanotubular structure of NT-700 collapses completely and so no cross section image is shown here.

2. Experimental details

2.1. Sample preparation

A NiTi alloy (50.8 at% Ni) rod (Xi'an Saite, China) was cut into thin sheets (Φ 14 mm × 2 mm), ground and polished to a mirror finish, sequentially ultrasonically cleaned in acetone, ethanol, and deionized water for 5 min each, and dried in cool air. Electrochemical anodization was carried out using a power supply (IT6121, ITECH, China) in the constant voltage mode. The NiTi sheet and platinum (Pt) foil (10 mm × 10 mm × 0.2 mm) were the anode and cathode, respectively. Anodization was conducted in 100 ml of the electrolyte composed of EG supplemented with 0.2 wt% NH_4F and 0.5 vol% H_2O at 30 °C and 25 V for 90 min to fabricate the Ni-Ti-O NTs. The as-anodized NTs were then annealed at 200 °C, 400 °C, 600 °C, or 700 °C for 2 h at a heating rate of 3 °C/min in a tubular annealing furnace. The samples were cooled to room temperature inside the furnace.

2.2. Sample characterization

The morphology of the samples was observed by field emission scanning electron microscopy (FE-SEM, JSM-7001F, JEOL) and the microstructure was determined by X-ray diffraction (XRD, DX-2700, Haoyuan, China). The data were collected in the 2θ range of 25–80° at an incident angle of 2°. The surface finish of all the samples were characterized using atomic force microscopy (AFM, SPA-300HV). The microstructure and composition of the samples was analyzed by transmission electron microscopy (TEM, JEM-2100F, JEOL) and selected area electron diffraction (SAED). Energy Dispersive Spectroscopy (EDS, Oxford, UK) was used to detect the distribution of Ni、Ti、O elements along the NTs. X-ray photoelectron spectrometry (XPS, K-Alpha, Thermo) was employed to determine the surface chemical composition and chemical states of the elements with the C1s (284.8 eV) peak used as the reference to calibrate the binding energies.

2.3. Ni release

To determine the nickel ion release rate from all the samples, each sample was immersed in 3 ml of phosphate buffered saline (PBS, pH = 7.4), which is composed of 137 mM NaCl, 2.7 mM KCl, 1.5 Mm KH_2PO_4, and 8 mM Na_2HPO_4 [25]. The solution was refreshed every day to mimic the *in vivo* dynamic environment and immersion continued for 30 days. The PBS containing the released Ni (three samples for each group) was sampled at time points of 1, 5, 10, 20 and 30 days and analyzed by inductively-coupled plasma mass spectroscopy (ICP-MS, Agilent 7500, Agilent).

2.4. Corrosion behavior

All electrochemical experiments were conducted on an electrochemical workstation (CS350, CorrTest, China) at 37 ± 0.5 °C with a conventional three-electrode cell to investigate the corrosion behavior of the samples. A saturated calomel electrode (SCE) was used as the reference electrode and a platinum (Pt) foil served as the counterpart. After each sample with an exposed area of 1 cm^2 was immersed in 100 ml of the PBS, open circuit potential (OCP) was recorded. After a total immersion time of 2 h, the potentiodynamic polarization was performed over a potential window of −0.8 V to 1.5 V relative to the SCE at a scanning rate of 1 mV/s. The corrosion potential (E_{corr}), corrosion current density (I_{corr}), and cathodic Tafel slope (β_c) of each sample were derived from the polarization curve by Tafel extrapolation.

2.5. Cytocompatibility

CCK-8 (Sangon) assay was used to evaluate the cytocompatibility of the samples. Before the experiments, all the samples were sterilized with 75 vol% alcohol for 30 min and rinsed with sterile PBS three times. The MC3T3-E1 osteoblasts were seeded on the sample surfaces at a density of 1 × 10^4 cells/cm^2 in a 24-well culture plate and cultured in α-DMEM (Gibco) containing 10 vol% fetal bovine serum (Sijiqing, China), 100 μg/ml streptomycin, and 100 units/ml penicillin in a humidified atmosphere with 5% CO_2 at 37 ± 0.1 °C. After culturing for 1, 3, and 5 days, all the samples were gently rinsed thrice with PBS and transferred to a new 24-well plate. Afterward, 100 μl of the CCK-8 solution and 900 μl of fresh culture medium were added to each well and incubated at 37 °C for 2 h. After incubation, 100 μl of the medium in each well was transferred to a 96-well plate and the absorbance was measured at 450 nm on a microplate reader (SM-3, TIANSHI).

3. Results

3.1. Sample characterization

The surface and cross-sectional FE-SEM images of the as-anodized and annealed samples are displayed in Fig. 1. NTs with a diameter of about 50 nm and length of about 700 nm are observed from the as-anodized sample (denoted as NT). After annealing at 200 °C (denoted as NT-200), 400 °C (denoted as NT-400), or 600 °C (denoted as NT-600), no surface and cross-sectional changes can be observed compared with NT. However, annealing at 700 °C (denoted as NT-700) results in complete structural collapse and so NT-700 is omitted from subsequent experiments.

Fig. 2 shows the AFM surface morphology of the NiTi control, as-anodized and annealed samples and their average surface roughness

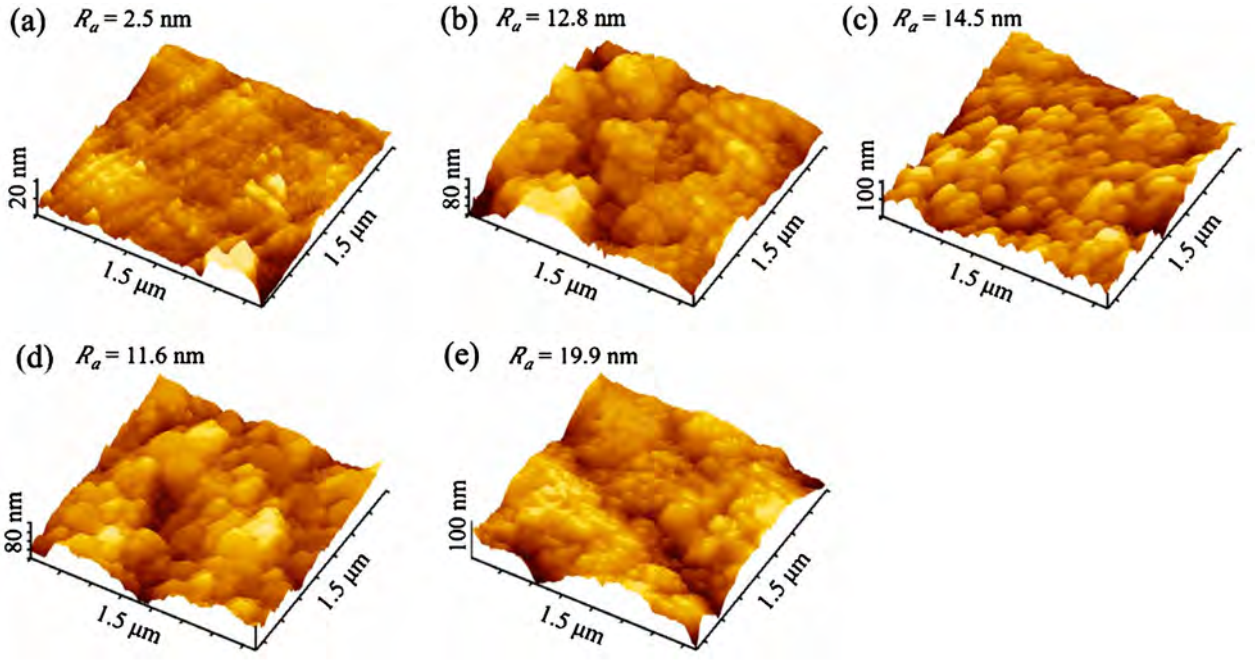

Fig. 2. Surface topography of the samples visualized by AFM. Their respective surface roughness values (R_s) are given in each image. (a) NiTi alloy, (b) NT, (c) NT-200, (d) NT-400, and (e) NT-600.

values (R_s) were calculated. The surface of NiTi control is very smooth and the roughness is only 2.5 nm. However, constructing nanotubular structure on its surface increases the R_s to 11.6–19.9 nm. No correlation can be found between annealing temperature and surface roughness of the anodized samples.

The XPS survey spectra acquired from the samples are shown in Fig. 3(a) and the corresponding quantitative results are summarized in Table 1. Ti, Ni, and O are the main elements in the NTs and C, N, and Si are adventitious contaminants. The ratios of Ni to Ti in the samples are less than that in the NiTi substrate implying preferential dissolution of Ni during anodization. Only a small amount of F can be detected on the as-anodized sample in spite of the use of the F-containing electrolyte indicating that annealing removes F from the NTs. Fig. 3(b) shows the high-resolution Ti 2p XPS spectra. There are two peaks at 458.8 eV and 464.4 eV are associated with Ti 2p3/2 and Ti 2p1/2 in TiO_2, respectively [25,26]. Fig. 3(c) displays the high-resolution Ni 2p XPS spectra and the Ni 2p3/2 and Ni 2p1/2 peaks at 855.6 and 873.6 eV, respectively, indicate that Ni is in the form of NiO and/or $Ni(OH)_2$ [20,27]. In addition, small fraction of NiF_2 (centered at 857.4 eV [28]) may be present in the as-anodized NTs because of the usage of F^- as an etching ion during anodization. However, annealing eliminate F species as verified by XPS survey spectra (Fig. 3(a)).

Table 1
Surface elemental concentrations (at%) of the Ni-Ti-O NTs determined by XPS.

Sample	Atomic concentrations (at%)							Ni/Ti ratio
	Ti	Ni	O	C	N	Si	F	
NT	9.47	2.15	31.95	50.01	1.65	2.24	2.53	0.23
NT-200	10.16	1.74	36.83	45.82	1.57	3.88	–	0.17
NT-400	13.33	2.08	51.02	22.12	1.38	10.07	–	0.16
NT-600	14.99	1.95	45.88	30.69	1.52	4.97	–	0.13

Fig. 4 displays the XRD patterns of the untreated control, as-anodized NTs, and annealed NTs showing two prominent peaks at 42.8° and 78° corresponding to the (110) and (211) planes of the NiTi substrate. After annealing at 600 °C, a weak peak corresponding to the (202) plane of the Ni_3Ti phase can be observed, but no TiO_2 peaks can be observed suggesting that the NTs after annealing retains the amorphous structure.

Fig. 5 shows the TEM results of as-anodized and annealed samples. Nanotubular structure can be clearly seen in each image. SAED patterns of as-anodized, 200 and 400 °C annealed samples show dim halos, which suggest they are amorphous. In contrast, SAED pattern of NT-600

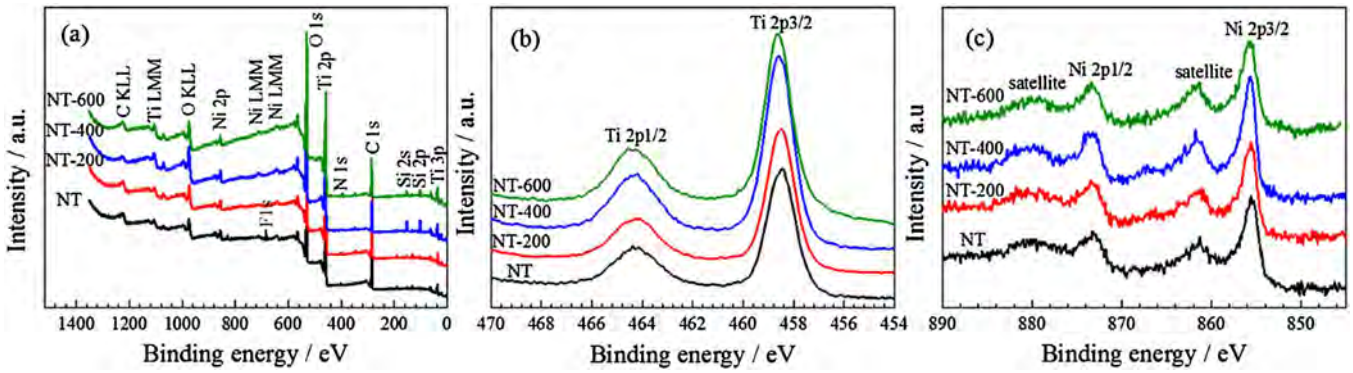

Fig. 3. (a) XPS survey spectra, (b) high-resolution Ti 2p spectra, and (c) high-resolution Ni 2p spectra acquired from the as-anodized and annealed Ni-Ti-O NTs.

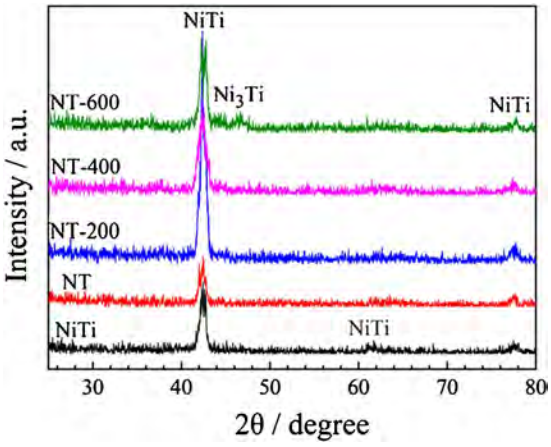

Fig. 4. XRD patterns of the NiTi control as well as as-anodized and annealed Ni-Ti-O NTs.

exhibits six relatively sharp diffraction rings, and the lattice spacings of 0.354, 0.246, 0.240, 0.190, 0.160, and 0.150 nm well match the (101), (103), (004), (200), (211), and (213) crystallographic planes of anatase respectively. However, anatase cannot be detected by XRD, which may be ascribed to its relatively weak signal intensity. EDS line scanning profiles show the constituent elements of Ni, Ti, and O are generally evenly distributed in all the NTs.

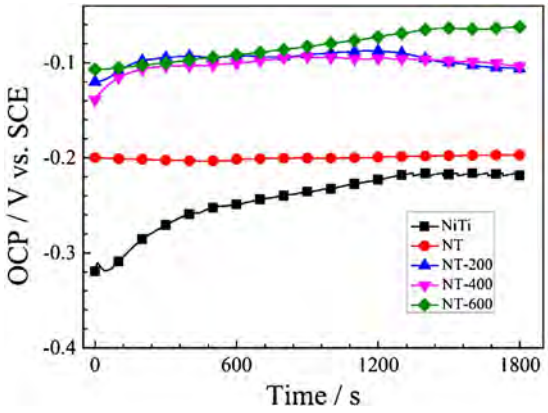

Fig. 6. Evolution of OCP with time recorded for the NiTi control, as-anodized and annealed NTs in PBS at 37 °C.

3.2. Corrosion behavior and Ni release

The evolution of OCP with time is shown in Fig. 6. For the NiTi control, the OCP value rises rapidly at the beginning, but then gradually slows and finally reaches a stable value around −0.22 V, which indicates a balance between formation and dissolution of the oxide film is established [29]. For NT, NT-200, NT-400, and NT-600, their OCP values finally stabilize at around −0.20 V, −0.11 V, −0.11 V and −0.06 V, respectively. Generally, the NTs show higher OCP values than

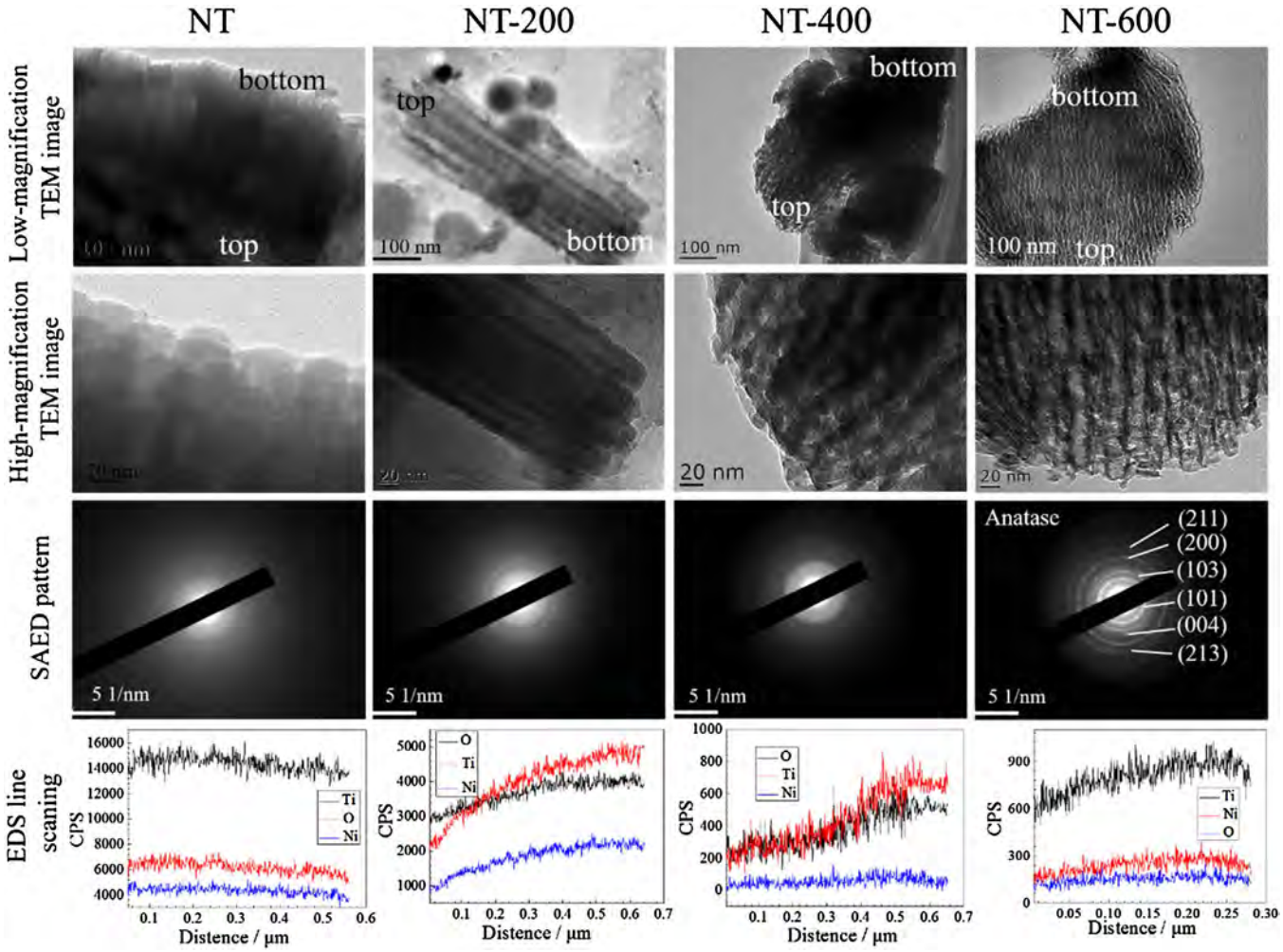

Fig. 5. TEM images, SAED patterns, and EDS line scanning profiles of the as-anodized and annealed Ni-Ti-O NTs. The direction of EDS line scanning is from top to bottom of the NTs shown in each low-magnification TEM image.

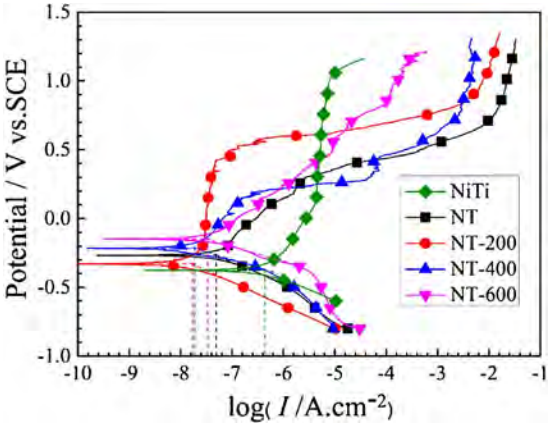

Fig. 7. Potentiodynamic polarization curves obtained from the NiTi control as well as as-anodized and annealed Ni-Ti-O NTs. The test was performed after the samples were immersed in PBS for 2 h at 37 °C.

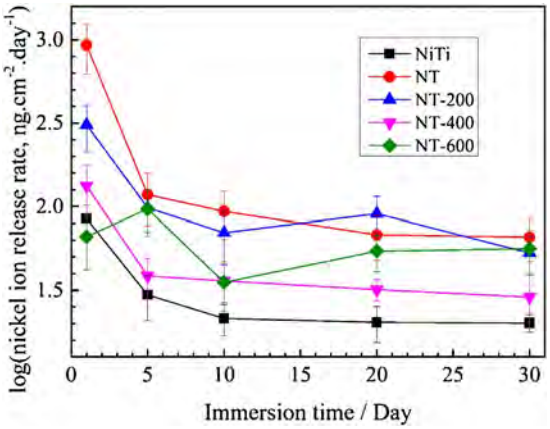

Fig. 8. Ni ion release rates from the NiTi control as well as as-anodized and annealed Ni-Ti-O NTs. The immersion solution for each sample was refreshed every day and each data means the average Ni ion release amount from each group over the day that it was measured. The scatter band represents standard deviation of three tests for each group.

the NiTi control and increasing annealing temperature contributes to the positive shift of OCP values.

Fig. 7 shows the potentiodynamic polarization curves of the NiTi control as well as as-anodized and annealed NTs. It can be seen that the cathodic polarization curves of all the samples exhibit Tafel (i.e., linear on semilogarithmic scale) over at least one decade of current density while the anodic branches show poor Tafel. Generally, the cathodic part reflects hydrogen evolution process through reduction of water, whereas the anodic region indicates the dissolution of the samples at an elevated potential. Passivation behavior is observed for the NiTi control and anodized samples show poor passivity except for NT-200 and NT-400. When the potential is higher than 0.5 V, no useful information that relevant to the system can be acquired. Based on these results, Tafel extrapolation was conducted using cathodic branches of the curves to determine the corrosion current densities. Since the extrapolation was started 50–100 mV away from E_{corr}, so the accuracy of the results can be anticipated [30,31]. The electrochemical parameters are presented in Table 2. Generally, the NTs show higher corrosion potentials and lower current densities than the NiTi control demonstrating that the NTs have high corrosion resistance. Generally, annealing can further lower the current densities and NT-200 and NT-400 show lower current densities than NT-600.

The Ni release profiles as a function of immersion time are presented in Fig. 8. Initially, relatively high Ni ion release rate can be observed for all the samples but afterwards, the release rate slows down with time finally reaching a steady state after 10 days. The as-anodized sample releases much more Ni than the other samples whereas the control releases a comparable amount of Ni as NT-400 and NT-600 in the initial stage.

3.3. Microstructure and chemical composition after immersion

The XPS results of the immersed samples are presented in Fig. 9 and the elemental compositions are listed in Table 3. Fig. 9(a) shows the presence of the main elements, Ti, Ni, and O, as well as contaminants, C, N, Si, P, and Ca. Generally, the ratios of Ni to Ti are smaller than those of the as-fabricated samples (Table 1), suggesting that Ni is more soluble than Ti during immersion. The locations of the Ti 2p and Ni 2p in Fig. 9(b) and (c) are the same as those of the as-fabricated ones (Fig. 3 (b) and (c)) indicating that immersion does not affect the chemical states.

Fig. 10 shows the XRD patterns of the samples after immersion in PBS for 30 days. Only peaks from the NiTi substrate can be detected from NT, NT-200, and NT-400. In addition, a peak corresponding to the (202) plane of Ni_3Ti can be observed from NT-600. In general, there is no appreciable difference between the as-fabricated (before immersion) (Fig. 4) and immersed (Fig. 10) samples providing evidence that the structure of the NTs are quite stable.

Table 2
Corrosion potentials (E_{corr}), current densities (I_{corr}), and cathodic Tafel slopes (β_c) of the NiTi control and Ni-Ti-O NTs derived from the polarization curves.

Sample	E_{corr}/V vs. SCE	I_{corr}/A cm^{-2}	βc/V decade^{-1}
NiTi	−0.38	4.40×10^{-7}	−0.162
NT	−0.27	4.90×10^{-8}	−0.158
NT-200	−0.33	1.70×10^{-8}	−0.173
NT-400	−0.22	1.69×10^{-8}	−0.111
NT-600	−0.15	3.33×10^{-8}	−0.111

3.4. Cytocompatibility

The osteoblasts viability cultured on all the sample surfaces was assayed using CCK-8 (Fig. 11). Generally, all the samples can well support cell growth throughout the whole culture period. There is no significant difference in cell viability between each group, which suggests the release levels of Ni can be tolerated by osteoblasts.

4. Discussion

During exposure to human body fluids, spontaneously electrochemical corrosion occurs on the surface of NiTi alloy resulting in continuous release of Ni ions from the bulk materials. This is commonly acknowledged to be the main reason that compromises the cytocompatibility. Accordingly, almost all previous works have aimed at inhibiting Ni release from the NiTi alloy by conducting various surface modification techniques [19,32–34]. Nonetheless, the relationship between Ni release and cytocompatibility is still ambiguous because these surface modification techniques not only reduce the Ni release, but also modify the surface morphology, microstructure, and chemical composition which may play important roles in the cytocompatibility as well.

In this work, we aim at elucidating the relationship between Ni release and cytocompatibility of the NiTi alloy. Ni-Ti-O NTs were prepared on the NiTi alloy by anodization followed by annealing at different temperature. The annealing temperature affects the morphology and microstructure of the NTs. It has been reported that amorphous TiO_2 NTs prepared by anodization of pure Ti can transform to anatase at 450 °C and rutile at 550 °C, eventually collapsing at a higher temperature because of the growth of the rutile phase [35,36]. However, the transformation temperature is elevated because of the presence of Ni in the Ni-Ti-O NTs. Previous work has shown that alloying elements such as tungsten (W) may elevate the phase transition

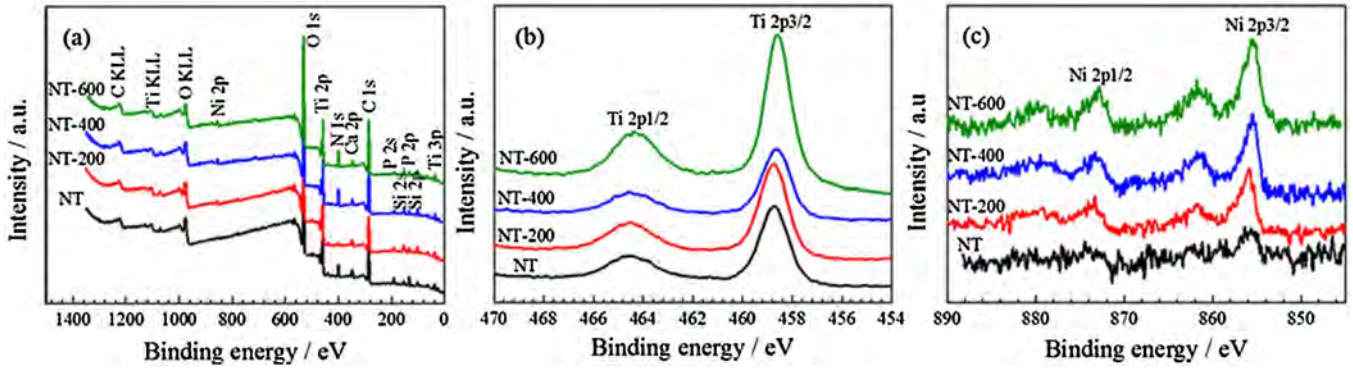

Fig. 9. (a) XPS survey spectra, (b) High-resolution Ti 2p spectra, and (c) High-resolution Ni 2p spectra of the as-anodized and annealed Ni-Ti-O NTs after immersion in PBS for 30 days.

Table 3
Surface elemental concentrations (at%) of the Ni-Ti-O NTs after immersion in PBS for 30 days determined by XPS.

Sample	Atomic concentrations (at%)								Ni/Ti ratio
	Ti	Ni	O	C	N	Si	P	Ca	
NT	5.68	0.68	38.93	37.54	5.37	4	5.81	1.99	0.12
NT-200	10.46	1.06	43.41	29.25	1.25	8.34	3.76	2.47	0.10
NT-400	5.28	0.81	34.43	44.07	6.2	5.13	2.88	1.21	0.15
NT-600	11.16	1.02	40.56	34.36	4.02	4.18	3.35	1.34	0.09

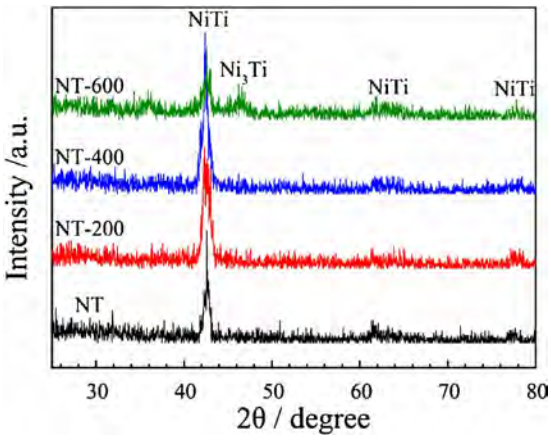

Fig. 10. XRD patterns of the as-anodized and annealed Ni-Ti-O NTs after immersion in PBS for 30 days.

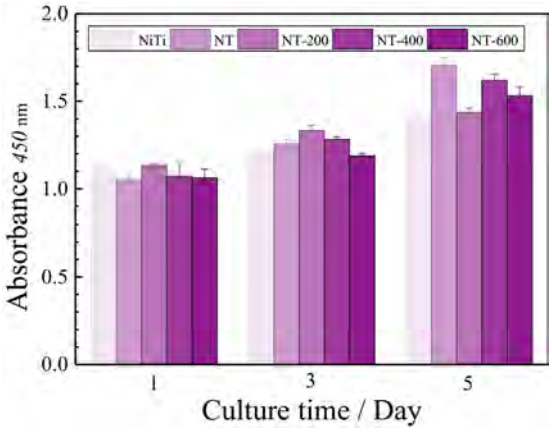

Fig. 11. Viability of osteoblasts after culturing on all the sample surfaces for 1, 3, and 5 days assayed by CCK-8.

temperature of TiO_2 NTs [37]. Another work demonstrated that when the NiTi alloy was annealed at 400 °C no crystalized TiO_2 could be detected on its surface, and annealing temperature of 600 °C could lead to the generation of anatase [38], which well matches our results.

The main reason accounts for Ni release from bulk NiTi alloy in an electrolyte is electrochemical corrosion, during which process metallic Ni converts to Ni^{2+} and releases into the electrolyte. The release rate of Ni^{2+} can be estimated by corrosion current density. In principle, low current density indicates high corrosion resistance and therefor little Ni release. However, the NiTi control shows the highest corrosion current but the amount of Ni released is less than those from the anodized samples, which result is consistent with previously reported one [39]. A possible explanation for the inconsistency between corrosion current and Ni release amount may be the polarization curves were measured only over a minutes, whereas the Ni release was over days. In the initial stage of immersion, the oxide film on NiTi control is relatively thin and cannot retard mass transport effectively as manifested by relatively high corrosion current when compared with that of anodized samples. As time goes on, the oxide film may grow gradually through the diffusion of oxygen to the substrate/oxide interface and formation of Ni and Ti oxides thus lowering Ni release rate [12]. As for the anodized samples, their corrosion currents are relatively low in the initial stage because of the presence of thick oxide films. Therefore, Ni release amount from anodized samples due to electrochemical corrosion is smaller than that from NiTi control. However, chemical dissolution of the Ni-containing NTs with large specific surface area may mainly account for the Ni release. In as-anodized NTs, Ni is in the form of Ni $(OH)_2$ and NiF_2, which are water-soluble [40]. Both the presence of water-soluble Ni species in the NTs and high corrosion current density may explain the highest Ni release level of the as-anodized NTs when compared with annealed samples. On one hand, annealing may convert NiF_2 to NiO [41], which is verified by the elimination of F after annealing (Fig. 3(a)), while NiO may then transform to slightly water-soluble $Ni(OH)_2$ after reacting with water [42]. On the other hand, annealing may further oxidize the NiTi substrate to thicken the surface oxide layer and therefore elevating the energy barrier for corrosion induced Ni ions release. These two factors may collectively lead to lower Ni release from annealed NTs. For NT-600, its corrosion current density is higher than that of NT-400, but their Ni release levels are comparable. Different crystal structure of the two samples may explain the phenomenon. Crystallization of the sample annealed at 600 °C may result in the incorporation of Ni in the NTs into the lattice of anatase thus reducing its chemical solubility when compared with that of annealed at 400 °C. Higher corrosion current density and lower chemical solubility of NT-600 than that of NT-400 may make them release Ni ions at the same level. Collectively, NT, NT-200, and NT-400 possess similar chemical composition, microstructure and morphology but release Ni ions at different levels thus an ideal platform to investigate the influence of Ni release on the cytocompatibility of the NiTi alloy. In addition, NT-400 and NT-600 possess similar chemical

composition, morphology and Ni release level but different microstructure, so the effect of microstructure on the cytocompatibility can be evaluated using the two groups as well.

There is no direct evidence to correlate the relationship between reduced Ni release and improved cytocompatibility, because after surface modification, the morphology, microstructure, and chemical composition of the NiTi alloy are altered [43]. Our results show even though the NTs release more Ni ions than NiTi control, they possess similar cytocompatibility, suggesting a certain amount of Ni can be tolerated by the cells. More importantly, the NTs (NT, NT-200, and NT-400) with similar morphology, microstructure, and chemical composition but different Ni release levels (132–929 ng/cm^2/day) show similar cytocompatibility, confirming that the cells can tolerate 929 ng/cm^2/day of Ni, which is significantly larger than that released from the untreated NiTi control (84.8 ng/cm^2/day). Accordingly, our results suggest that the strategy to improve the cytocompatibiliy of NiTi should consider the surface morphology, microstructure, and chemical composition instead of just focusing on the amount of released Ni.

5. Conclusion

Ni-Ti-O NTs annealed at 200–400 °C possess nanotubular morphology, amorphous microstructure, and similar chemical composition as the as-anodized sample. In contrast, annealing at 600 °C converts the amorphous microstructure to anatase. Generally, the NTs have better corrosion resistance but release more Ni ions than the untreated NiTi control, suggesting that chemical dissolution of Ni species in the NTs also accounts for the Ni release. Nonetheless, the NTs and NiTi control possess comparable cytocompatibility. In addition, the anodized samples with similar surface characteristics and different Ni release levels also show similar cytocompatibility, indicating that the amount of Ni released from the NTs are tolerated by the cells. Accordingly, the cytocomatibility of the NiTi alloy should be improved by altering the surface morphology, microstructure, and chemical composition rather than simply reducing Ni release.

Acknowledgments

This work was jointly supported by the National Natural Science Foundation of China (31400815), Scientific and Technological Innovation Programs of Higher Education Institutions of Shanxi (201626), Hong Kong Research Grants Council (RGC) General Research Funds (GRF) No. CityU 11301215, and City University of Hong Kong Applied Research Grant (ARG) No. 9667122.

References

[1] S.A. Bernard, V.K. Balla, N.M. Davies, S. Bose, A. Bandyopadhyay, Bone cell-materials interactions and Ni ion release of anodized equiatomic NiTi alloy, Acta Biomater. 7 (4) (2011) 1902–1912.
[2] K. Asami, S.-C. Chen, H. Habazaki, K. Hashimoto, The surface characterization of titanium and titanium-nickel alloys in sulfuric acid, Corros. Sci. 35 (1–4) (1993) 43–49.
[3] X. Liu, S. Wu, K.W.K. Yeung, Y.L. Chan, T. Hu, Z. Xu, X. Liu, J.C.Y. Chung, K.M.C. Cheung, P.K. Chu, Relationship between osseointegration and superelastic biomechanics in porous NiTi scaffolds, Biomaterials 32 (2) (2011) 330–338.
[4] D.O. Flamini, M. Saugo, S.B. Saidman, Electrodeposition of polypyrrole on Nitinol alloy in the presence of inhibitor ions for corrosion protection, Corros. Sci. 81 (2014) 36–44.
[5] R. Hang, S. Ma, V. Ji, P.K. Chu, Corrosion behavior of NiTi alloy in fetal bovine serum, Electrochim. Acta 55 (20) (2010) 5551–5560.
[6] E. Denkhaus, K. Salnikow, Nickel essentiality, toxicity, and carcinogenicity, Crit. Rev. Oncol. Hematol. 42 (1) (2002) 35–56.
[7] C.W. Chan, H.C. Man, T.M. Yue, Susceptibility to stress corrosion cracking of NiTi laser weldment in Hanks' solution, Corros. Sci. 57 (2012) 260–269.
[8] K. Fushimi, M. Startmann, A.W. Hassel, Electropolishing of NiTi shape memory alloys in methanolic H_2SO_4, Electrochim. Acta 52 (3) (2006) 1290–1295.
[9] S. Barison, S. Cattarin, S. Daolio, M. Musiani, A. Tuissi, Characterisation of surface oxidation of nickel-titanium alloy by ion-beam and electrochemical techniques, Electrochim. Acta 50 (1) (2004) 11–18.
[10] F. Villermaux, M. Tabrizian, L.H. Yahi, M. Meunier, D.L. Piron, Excimer laser treatment of NiTi shape memory alloy biomaterials, Appl. Surf. Sci. 109–110 (1997) 62–66.
[11] S.A. Shabalovskaya, J. Anderegg, F. Laabs, P.A. Thiel, G. Rondelli, Surface conditions of Nitinol wires, tubing, and as-cast alloys. The effect of chemical etching, aging in boiling water, and heat treatment, J. Biomed. Mater. Res. B 65 (1) (2003) 193–203.
[12] G.S. Firstov, R.G. Vitchev, H. Kumar, B. Blanpain, J.V. Humbeeck, Surface oxidation of NiTi shape memory alloy, Biomaterials 23 (24) (2002) 4863–4871.
[13] K.W.K. Yeung, R.W.Y. Poon, X.M. Liu, P.K. Chu, C.Y. Chung, X.Y. Liu, S. Chan, W.W. Lu, D. Chan, K.D.K. Luk, K.M.C. Cheung, Nitrogen plasma-implanted nickel titanium alloys for orthopedic use, Surf. Coat. Technol. 201 (9–11) (2007) 5607–5612.
[14] K.W.K. Yeung, R.Y.L. Chan, K.O. Lam, S.L. Wu, X.M. Liu, C.Y. Chung, P.K. Chu, W.W. Lu, D. Chan, K.D.K. Luk, K.M.C. Cheung, In vitro and in vivo characterization of novel plasma treated nickel titanium shape memory alloy for orthopedic implantation, Surf. Coat. Technol. 202 (4–7) (2007) 1247–1251.
[15] Y.L. Chan, S.L. Wu, X.M. Liu, P.K. Chu, K.W.K. Yeung, W.W. Lu, A.H.W. Ngan, K.D.K. Luk, D. Chan, K.M.C. Cheung, Mechanical properties, bioactivity and corrosion resistance of oxygen and sodium plasma treated nickel titanium shape memory alloy, Surf. Coat. Technol. 202 (4–7) (2007) 1308–1312.
[16] R.W.Y. Poon, J.P.Y. Ho, X. Liu, C.Y. Chung, P.K. Chu, K.W.K. Yeung, W.W. Lu, K.M.C. Cheung, Anti-corrosion performance of oxidized and oxygen plasma-implanted NiTi alloys, Mater. Sci. Eng. A 390 (1-2) (2005) 444–451.
[17] C.L. Chu, T. Hu, S.L. Wu, Y.S. Dong, L.H. Yin, Y.P. Pu, P.H. Lin, C.Y. Chung, K.W. Yeung, P.K. Chu, Surface structure and properties of biomedical NiTi shape memory alloy after Fenton's oxidation, Acta Biomater. 3 (5) (2007) 795–806.
[18] Z.D. Cui, H.C. Man, X. Yang, The corrosion and nickel release behavior of laser surface-melted NiTi shape memory alloy in Hanks' solution, Surf. Coat. Technol. 192 (2-3) (2005) 347–353.
[19] R. Hang, M. Zhang, S. Ma, P.K. Chu, Biological response of endothelial cells to diamond-like carbon-coated NiTi alloy, J. Biomed. Mater. Res. A 100 (2) (2012) 496–506.
[20] J.-H. Kim, K. Zhu, Y. Yan, C.L. Perkins, A.J. Frank, Microstructure and pseudocapacitive properties of electrodes constructed of oriented NiO-TiO_2 nanotube arrays, Nano Lett. 10 (10) (2010) 4099–4104.
[21] R. Hang, A. Gao, X. Huang, X. Wang, X. Zhang, Q. Lin, B. Tang, Antibacterial activity and cytocompatibility of Cu-Ti-O nanotubes, J. Biomed. Mater. Res. A 102 (6) (2014) 1850–1858.
[22] L. Bai, R. Wu, Y. Wang, X. Wang, X. Zhang, X. Huang, L. Qin, R. Hang, L. Zhao, B. Tang, Osteogenic and angiogenic activities of silicon-incorporated TiO_2 nanotube arrays, J. Mater. Chem. B 4 (2016) 5548–5559.
[23] A. Gao, R. Hang, X. Huang, L. Zhao, X. Zhang, L. Wang, B. Tang, S. Ma, P.K. Chu, The effects of titania nanotubes with embedded silver oxide nanoparticles on bacteria and osteoblasts, Biomaterials 35 (13) (2014) 4223–4235.
[24] R. Hang, Y. Liu, L. Zhao, A. Gao, L. Bai, X. Huang, X. Zhang, B. Tang, P.K. Chu, Fabrication of Ni-Ti-O nanotube arrays by anodization of NiTi alloy and their potential applications, Sci. Rep.-UK (2014) 7547.
[25] R. Hang, Y. Liu, S. Liu, L. Bai, A. Gao, X. Zhang, X. Huang, B. Tang, P.K. Chu, Size-dependent corrosion behavior and cytocompatibility of Ni-Ti-O nanotubes prepared by anodization of biomedical NiTi alloy, Corros. Sci. 103 (2016) 173–180.
[26] N. Ohtsu, K. Sakamoto, Y. Hirano, M. Yamane, XPS analysis of a heat-treated NiTi surface for elucidating Ni segregation phenomena, Surf. Interface Anal. 48 (7) (2016) 488–492.
[27] R. Hang, Y. Liu, A. Gao, L. Bai, X. Huang, X. Zhang, N. Lin, B. Tang, P.K. Chu, Highly ordered Ni-Ti-O nanotubes for non-enzymatic glucose detection, Mater. Sci. Eng. C 51 (2015) 37–42.
[28] M. Jin, G. Zhang, F. Yu, W. Li, W. Lu, H.T. Huang, Sponge-like $Ni(OH)_2$-NiF_2 composite film with excellent electrochemical performance, Phys. Chem. Chem. Phys. 15 (2013) 1601–1605.
[29] Y. Li, H. Zhang, X. Wang, J. Lia, F. Wang, Growth kinetics of oxide films at the polyaniline/mild steel interface, Corros. Sci. 53 (12) (2011) 4044–4049.
[30] O. Dolgikh, A.C. Bastos, A. Oliveira, C. Dan, J. Deconinck, Influence of the electrolyte film thickness and NaCl concentration onthe oxygen reduction current on platinum, Corros. Sci. 102 (2016) 338–347.
[31] E. McCafferty, Validation of corrosion rates measured by the Tafel extrapolation method, Corros. Sci. 47 (12) (2005) 3202–3215.
[32] J. Li, G. Wang, H. Geng, H. Zhu, M. Zhang, Z. Di, X. Liu, P.K. Chu, X. Wang, CVD growth of graphene on NiTi alloy for enhanced biological activity, ACS Appl. Mater. Interfaces 7 (36) (2015) 19876–19881.
[33] X. Liu, Z. Weng, P. Li, H.M. Wong, W. Wang, S. Wu, K.W.K. Yeung, P.K. Chu, Enhanced bioactivity of biomedical NiTi through surface plasma polymerization, Nanosci. Nanotechnol. Lett. 7 (3) (2015) 220–225.
[34] S. Shabalovskaya, J. Anderegg, J.V. Humbeeck, Critical overview of nitinol surfaces and their modifications for medical applications, Acta Biomater. 4 (3) (2008) 447–467.
[35] Y. Sun, K. Yan, G. Wang, W. Guo, T. Ma, Effect of annealing temperature on the hydrogen production of TiO_2 nanotube arrays in a two-compartment photoelectrochemical cell, J. Phys. Chem. C 115 (26) (2011) 725–733.
[36] O.K. Varghese, D. Gong, M. Paulose, Crystallization and high-temperature structural stability of titanium oxide nanotube arrays, J. Mater. Res. 18 (1) (2003) 156–165.
[37] Y.-C. Nah, A. Ghicov, D. Kim, S. Berger, P. Schmuki, TiO_2-WO_3 compositenanotubes by alloy anodization: growth and enhanced electrochromic properties, J. Am. Chem. Soc. 130 (2008) 16154–16155.
[38] Y. Gu, B. Tay, C. Lim, M. Yong, Characterization of bioactive surface oxidation layer on NiTi alloy, Appl. Surf. Sci. 252 (5) (2005) 2038–2049.

[39] P.P. Lee, A. Cerchiari, T. Desai, Nitinol-based nanotubular coatings for the modulation of human vascular cell function, Nano Lett. 14 (9) (2014) 5021–5028.
[40] D. Meyer, J.M. Birdsey, M. Wendolowski, K.K. Dobbin, P.L. Williams, Differential toxicities of nickel salts to the nematode caenorhabditis elegans, Bull. Environ. Contam. Toxicol. 97 (2016) 166–170.
[41] L. Wang, G. Zhang, Y. Liu, W. Li, W. Lu, H.T. Huang, Facile synthesis of a mechanically robust and highly porous NiO film with excellent electrocatalytic activity towards methanol oxidation, Nanoscale 8 (2016) 11256–11263.
[42] X. Dai, D. Chen, H. Fan, Y. Zhong, L. Chang, H. Shao, J. Wang, J. Zhang, C. Cao, Ni $(OH)_2$/NiO/Ni composite nanotube arrays for high-performance supercapacitors, Electrochim. Acta 154 (2015) 128–135.
[43] N.K. Allam, C.A. Grimes, Formation of vertically oriented TiO_2 nanotube arrays using a fluoride free HCl aqueous electrolyte, J. Phys. Chem. C 111 (35) (2007) 13028–13032.